JOURNAL OF ENERGY, MATERIALS, AND INSTRUMENTATION TECHNOLOGY

Journal Webpage https://jemit.fmipa.unila.ac.id/

Immobilization of Tungsten Oxide (WO_3) Material on Glass Substrate Using the Direct Spray Deposition (DSD)

Iqbal Firdaus[1*], Hendri Widyandari[2], Pulung Karo Karo[1], Rana Yuliandra[1], and Yusril Al Fath[1]

1. Department of Physics, Faculty of Mathematics and Natural Sciences, University of Lampung, Bandar Lampung, 35145, Indonesia
2. Department of Physics, Faculty of Mathematics and Natural Sciences, Universitas Sebelas Maret, Surakarta, 57126, Indonesia

Article Information

Article history:
Received April 25, 2026
Received in revised form May 22, 2026
Accepted May 23, 2026

Keywords: *Tungsten Oxide (WO_3), Direct Spray Deposition (DSD), Annealing, Glass*

Abstract

Tungsten oxide (WO_3) is a semiconductor material with promising potential for photocatalytic applications due to its visible-light response and good chemical stability. In this study, WO_3 films were successfully immobilized on glass substrates using a combination of photodeposition and Direct Spray Deposition (DSD) methods. The precursor solution was prepared from ammonium paratungstate, followed by photodeposition under visible-light irradiation and deposition onto heated glass substrates using the DSD technique. The deposited films were annealed at temperatures of 500 °C, 600 °C, and 650 °C. Structural characterization was performed using X-Ray Diffraction (XRD), while surface morphology was analyzed using Scanning Electron Microscopy (SEM). XRD results revealed that increasing the annealing temperature improved the crystallinity of the films and induced phase transformations from W_5O_{14} to $W_{25}O_{73}$ and $W_{18}O_{49}$ phases. SEM observations showed that higher annealing temperatures produced denser and more uniform film surfaces, with plate-like morphologies clearly observed at 650 °C. These findings demonstrate that annealing temperature strongly influences the structural and morphological characteristics of WO_3 films prepared by the DSD method.

Informasi Artikel

Proses artikel:
Diterima 23 April 2026
Diterima dan direvisi dari 20 Mei 2026
Accepted 25 Mei 2026

Kata kunci: *Tungsten Oksida (WO_3), Direct Spray Deposition (DSD), Annealing, Kaca*

Abstrak

Tungsten oksida (WO_3) merupakan material semikonduktor yang memiliki potensi besar untuk aplikasi fotokatalis karena responsnya terhadap cahaya tampak dan stabilitas kimia yang baik. Pada penelitian ini, film WO_3 berhasil diimobilisasi pada substrat kaca menggunakan kombinasi metode fotodeposisi dan Direct Spray Deposition (DSD). Larutan prekursor dibuat dari ammonium paratungstate, kemudian dimodifikasi melalui proses fotodeposisi di bawah penyinaran cahaya tampak dan dilapiskan pada substrat kaca yang dipanaskan menggunakan teknik DSD. Film yang dihasilkan kemudian diannealing pada suhu 500 °C, 600 °C, dan 650 °C. Karakterisasi struktur kristal dilakukan menggunakan X-Ray Diffraction (XRD), sedangkan morfologi permukaan dianalisis menggunakan Scanning Electron Microscopy (SEM). Hasil XRD menunjukkan bahwa peningkatan suhu annealing meningkatkan kristalinitas film dan memicu transformasi fase dari W_5O_{14} menjadi $W_{25}O_{73}$ dan $W_{18}O_{49}$. Hasil SEM menunjukkan bahwa peningkatan suhu annealing menghasilkan permukaan film yang lebih padat dan seragam, serta membentuk morfologi menyerupai plate pada suhu 650 °C. Hasil penelitian menunjukkan bahwa suhu annealing berpengaruh signifikan terhadap karakteristik struktur dan morfologi film WO_3 yang disintesis menggunakan metode DSD.

* Corresponding author.
E-mail address: iqbal.firdaus@fmipa.unila.ac.id

1. Introduction

Industrial development has significantly contributed to environmental pollution, particularly water contamination caused by organic waste that is difficult to degrade. Several reports have shown that rivers surrounding industrial areas in Indonesia contain suspended solids of up to 750 mg/L and Biological Oxygen Demand (BOD) values reaching 500 mg/L. Conventional treatment methods, such as chemical oxidation, physical adsorption, and biological degradation, still exhibit several limitations due to their low effectiveness in decomposing complex organic compounds and their potential to generate hazardous by-products with relatively high operational costs (Cao et al., 2018). Therefore, alternative methods that are more effective, economical, and environmentally friendly are urgently required for wastewater treatment. One of the most widely developed technologies is photocatalysis, a semiconductor-based process categorized as an advanced oxidation process (AOP). In this process, semiconductor materials absorb light energy and generate electron–hole pairs, which subsequently produce reactive radicals such as hydroxyl radicals (OH*) capable of oxidizing organic pollutants into simpler compounds (Sarteep et al., 2016). Photocatalytic technology is considered highly effective because it can degrade organic pollutants without producing significant secondary pollutants.

Various metal oxide semiconductor materials, including TiO_2, WO_3, SnO_2, Bi_2O_3, and ZnO, have been reported to exhibit promising photocatalytic activity (Arutanti et al., 2022; Astuti et al., 2020; Widiyandari et al., 2012) . Among these materials, TiO_2 is the most extensively utilized due to its excellent chemical stability and high photocatalytic performance. However, TiO_2 possesses a relatively wide band gap of approximately 3.0–3.2 eV, limiting its activity primarily to the ultraviolet region (Xu et al., 2011; Yu et al., 2013). Various approaches, such as elemental doping and heterojunction engineering, have been explored to improve the visible-light response of TiO_2, although the resulting efficiency remains limited (Acevedo-Peña & González, 2014; Lee et al., 2020; Luo et al., 2009; Wang et al., 2009).

Tungsten oxide (WO_3) is an n-type semiconductor with a narrower band gap of approximately 2.4–2.8 eV, enabling light absorption within the visible-light region (Nagarjuna et al., 2017; Widiyandari et al., 2014). These characteristics make WO_3 a promising photocatalytic material for the degradation of organic pollutants under sunlight or domestic visible-light irradiation. In addition, WO_3 exhibits good chemical stability and has been applied in various fields, including energy conversion and wastewater treatment (Murillo-Sierra et al., 2021). The application of WO_3 as a photocatalytic material is generally carried out in the form of particles or thin films. The use of particulate photocatalysts often presents challenges in separating the catalyst material from the treated solution after the degradation process. Therefore, the development of WO_3 in thin-film form on solid substrates offers a more practical alternative. One potential technique is Direct Spray Deposition (DSD), a simple deposition method that enables the formation of material coatings on glass substrates through a relatively rapid and low-cost process.

Based on this background, this study focuses on the immobilization of tungsten oxide (WO_3) material on a glass substrate using the Direct Spray Deposition (DSD) method. Material characterization was performed using X-Ray Diffraction (XRD) to identify the crystal structure and Scanning Electron Microscopy (SEM) to observe the surface morphology of the deposited films. This study is expected to provide information regarding the structural and morphological characteristics of WO_3 films prepared using the DSD method.

2. Research Methods

2.1 Preparation of WO_3 Precursor Solution

A 0.01 M ammonium paratungstate precursor solution was prepared using ammonium paratungstate (purity 99.99%; molecular weight = 3060 g/mol). Approximately 3.081 g of ammonium paratungstate was dissolved in 100 mL of distilled water. The solution was then heated and stirred using a hot plate stirrer at 40 °C for approximately 20 min until a homogeneous solution was obtained.

2.2 Photodeposition of WO_3

The ammonium paratungstate solution was subsequently transferred into a photodeposition reactor maintained at 25 °C under visible-light irradiation from a halogen lamp (**Figure 1**). During the photodeposition process, 15 mL of methanol was added to the precursor solution, followed by irradiation for 3 h. After photodeposition, the methanol was removed by heating the solution at 65 °C for 2 h.

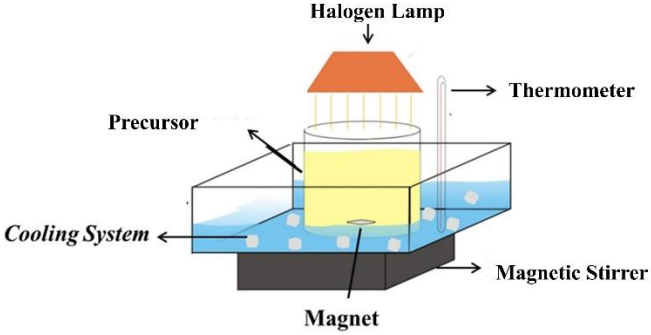

Figure 1. Photodeposition Process

2.3 Fabrication of WO_3 Thin Films

Substrate Cleaning

Glass substrates with dimensions of 7.5 cm × 2.5 cm were cleaned prior to deposition. The substrates were first immersed in acetone and treated using an ultrasonic cleaner at 40 °C for 20 min. Subsequently, the substrates were immersed in methanol and ultrasonically cleaned at 40 °C for 5 min. The same procedure was repeated using distilled water for another 5 min. Finally, the cleaned substrates were dried using compressed air.

Direct Spray Deposition (DSD)

The WO_3 films were fabricated using the Direct Spray Deposition (DSD) technique. A glass substrate (7.5 cm × 2.5 cm) was placed on a temperature-controlled hot plate maintained at 150 °C (**Figure 2**). Approximately 25 mL of the precursor solution was loaded into a spray gun and sprayed onto the heated glass substrate. After deposition, the coated films were allowed to cool naturally to room temperature. The deposited films were subsequently calcined in a furnace at temperatures of 500 °C, 600 °C, and 650 °C for 2 h to promote crystal formation.

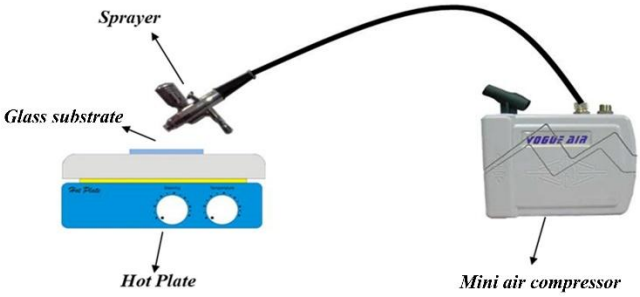

Figure 2. Schematic illustration of the WO_3 coating process

3. Results and Discussions

3.1 WO_3 Films Deposited on Glass Substrates

WO_3 films were successfully deposited onto glass substrates using a combination of photodeposition and Direct Spray Deposition (DSD) methods. The photodeposition process was employed to modify the WO_3 precursor solution, while the DSD technique was utilized for film coating on the glass substrates. The deposited films were subsequently characterized using X-Ray Diffraction (XRD) to investigate their crystal structure and phase composition, while Scanning Electron Microscopy (SEM) was employed to observe the surface morphology of the WO_3 films. The deposited WO_3 films are presented in **Figure 3**.

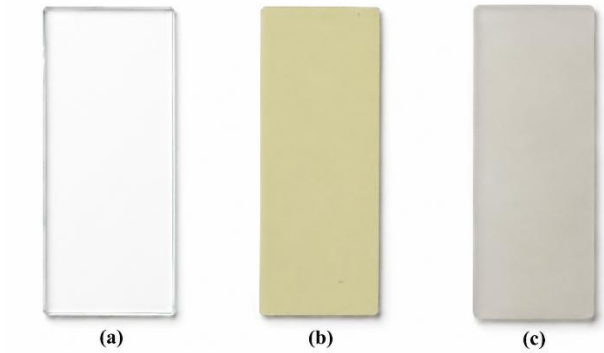

Figure 3. WO_3 films deposited on glass substrates at annealing temperatures of (a) 500 °C, (b) 600 °C, and (c) 650 °C.

3.2 Crystal Structure Analysis of WO_3 Films

The crystal structure of the deposited films was analyzed using XRD characterization. **Figure 4** shows the XRD patterns of WO_3 films annealed at temperatures of 500 °C, 600 °C, and 650 °C. Phase identification was carried out using HighScore Plus software.

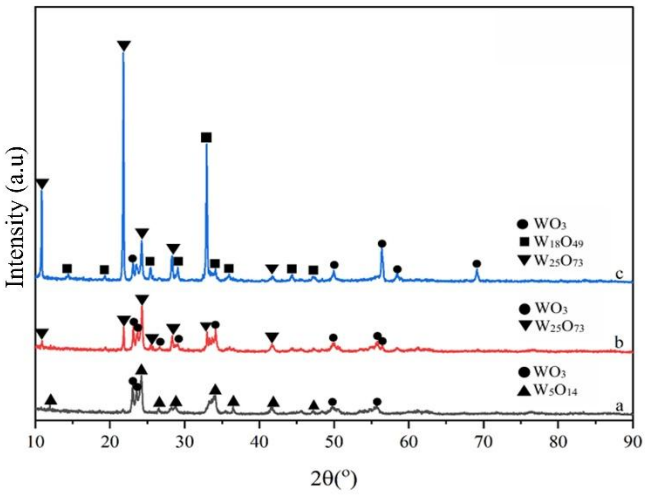

Figure 4. XRD patterns of WO_3 films at annealing temperatures of (a) 500 °C, (b) 600 °C, and (c) 650 °C

The crystal phases of tungsten oxide (WO_3) films were analyzed within the 2θ range of 10°–90°. The XRD results indicate that the annealing temperature plays an important role in influencing the phase transformation and crystallinity of the deposited films. At an annealing temperature of 500 °C (**Figure 4.a**), diffraction peaks corresponding to tungsten oxide phases W_5O_{14} and WO_3 were observed with relatively low intensity and broad peak characteristics, indicating incomplete crystallization. The WO_3 phase was identified as having a tetragonal crystal system with lattice parameters of a = 5.2806 Å, b = 5.2806 Å, and c = 7.8496 Å (ICDD 01-089-4482). Meanwhile, the W_5O_{14} phase exhibited a tetragonal crystal system with lattice parameters of a = 23.3300 Å, b = 23.3300 Å, and c = 3.7970 Å (ICDD 00-041-0745). The diffraction peaks located at 2θ values of 11.94°, 26.34°, 28.51°, 33.20°, and 34.06° were attributed to the (310), (311), (331), and (611) crystal planes of W_5O_{14}. In addition, peaks observed at 22.64°, 23.81°, 33.93°, and 41.17° indicated the presence of the WO_3 phase corresponding to the (002) and (110) crystal planes. At this temperature, the W_5O_{14} phase remained dominant, while several WO_3 peaks had already appeared, suggesting that the material was still undergoing phase transition from mixed tungsten oxide phases toward WO_3 formation.

Table 1. Identification of XRD Peaks

Sample	Crystal Peak	Ref.code ICDD	2θ (°)	Hkl
XRD 01-500 C	Tungsten oxide (W_5O_{14})	00-041-0745	11.94; 26.34; 28.51; 33.20; 34.06;	(310); (311); (331); (611); (541)
	Tungsten oxide (WO_3)	01-089-4482	22.64; 23.81; 33.93; 41.17; 46.22; 49.51; 54.94	(002); (110); (200); (202); (004); (104); (310)
XRD 02-600 C	Tungsten oxide ($W_{25}O_{73}$)	01-071-0070	10.83; 21.75; 23.27; 25.15; 28.23; 32.77; 41.64; 44.57; 45.07; 47.25; 48.61	(-106); (-2012); (010); (113); (-1110); (-315); (-3119); (-2124); (0125);
	Tungsten oxide (WO_3)	01-089-4482	23.81; 28.31; 49.51; 52.65; 54.94; 57.32	(516); (-4122) (110); (102); (104); (114); (310); (302)
XRD 03-650 C	Tungsten oxide ($W_{25}O_{73}$)	01-071-0070	10.83; 21.75; 23.27; 28.23; 41.70	(-106); (-2012); (010); (-1110); (2024)
	Tungsten oxide ($W_{18}O_{49}$)	03-065-1291	14.49; 23.45; 25.40; 29.05; 33.27; 33.61; 39.95; 44.98; 46.13	(-301); (010); (-204); (112); (-105); (113); (-315); (-902); (-216);
	Tungsten oxide (WO_3)	01-089-4482	23.81; 49.51; 54.94; 58.56; 69.43	(110); (104); (310); (204); (224)

When the annealing temperature was increased to 600 °C (**Figure 4.b**), sharper and more intense diffraction peaks were observed, indicating improved crystallinity. At this temperature, the $W_{25}O_{73}$ phase began to appear. This phase possesses a monoclinic crystal structure with lattice parameters of a = 11.9300 Å, b = 3.8200 Å, and c = 59.7200 Å (ICDD 01-071-0070). Characteristic diffraction peaks of $W_{25}O_{73}$ were identified at 2θ values of 10.83°, 21.75°, 23.27°, and 28.23°. In addition, the WO_3 phase became more pronounced, as indicated by peaks at 23.81°, 28.31°, and 49.51°. These results suggest a more significant phase transformation compared to the sample annealed at 500 °C. The increased peak intensity and sharper diffraction features indicate that the crystal structure became more ordered as the annealing temperature increased. At this stage, the W_5O_{14} phase was no longer dominant and had partially transformed into $W_{25}O_{73}$ and WO_3 phases.

At an annealing temperature of 650 °C (**Figure 4.c**), the diffraction patterns were dominated by $W_{25}O_{73}$ (ICDD 01-071-0070) and $W_{18}O_{49}$ (ICDD 03-065-1291) phases. Diffraction peaks located at 2θ values of 14.49°, 23.45°, 25.40°, and 29.05° corresponded to the ($\bar{3}01$), (010), ($\bar{2}04$), and (112) crystal planes, respectively. The WO_3 phase was still detected, although with lower peak intensity, indicating that higher annealing temperatures promoted the formation of more complex tungsten oxide phases such as $W_{18}O_{49}$. The $W_{18}O_{49}$ phase exhibits a monoclinic crystal

structure with lattice parameters of a = 18.3200 Å, b = 3.7900 Å, and c = 14.0400 Å. Additional diffraction peaks appearing at 33.27° and 33.61° further confirmed the presence of this phase. Overall, increasing the annealing temperature improved the crystallinity of the films and induced significant phase transformations from W_5O_{14} at lower temperatures toward $W_{25}O_{73}$ and $W_{18}O_{49}$ phases at higher temperatures. These results indicate that the WO_3 films underwent structural evolution during the annealing process, leading to the formation of more thermodynamically stable tungsten oxide phases at elevated temperatures.

Table 2. FWHM, crystallite size, dislocation density, and microstrain calculated from the main diffraction peak at 2θ ≈ 23°

Sample		2θ (°)	FWHM (°)	Crystallite Size (nm)	Dislocation Density (×10^14 lines/m²)	Microstrain (×10^-3)
XRD C	01-500	23.81	0.188	43.12	5.38	3.71
XRD C	02-600	23.27	0.141	57.51	3.02	2.77
XRD C	03-650	23.45	0.174	46.60	4.60	3.43

The crystallite size calculated using the Scherrer equation showed a strong dependence on calcination temperature. The sample calcined at 600 °C exhibited the largest crystallite size of 57.51 nm. This result indicates that crystal growth became more effective as the calcination temperature increased from 500 °C to 600 °C. The narrower diffraction peak observed at around 2θ ≈ 23° also confirmed the improvement in crystallinity. In contrast, the sample calcined at 500 °C showed a smaller crystallite size of 43.12 nm. The broader diffraction peak suggested that the crystallization process was not fully developed at lower temperature. Insufficient thermal energy limited atomic diffusion during crystal growth, resulting in smaller crystallites and a less ordered structure. A slight decrease in crystallite size was observed for the sample calcined at 650 °C. The crystallite size decreased to 46.60 nm, accompanied by an increase in peak broadening. This behavior may be associated with the formation of mixed tungsten oxide phases and the development of lattice distortion at higher calcination temperature.

The dislocation density values were inversely related to the crystallite size. The XRD 02-600 C sample exhibited the lowest dislocation density value of 3.02 ×10^14 lines/m², indicating a lower concentration of crystal defects and a more ordered crystal structure. Meanwhile, the XRD 01-500 C sample showed the highest dislocation density value, suggesting that structural imperfections were still dominant in the material. A similar trend was observed for the microstrain values. The lowest microstrain was obtained for the XRD 02-600 C sample, indicating reduced lattice distortion and improved crystal stability. On the other hand, the higher microstrain values observed for the 500 °C and 650 °C samples indicated the presence of internal strain within the crystal lattice. Overall, the XRD 02-600 C sample demonstrated the best crystal quality among all samples. This conclusion was supported by the combination of the largest crystallite size, the lowest dislocation density, and the smallest microstrain value. These results suggest that 600 °C is the optimum calcination temperature for producing tungsten oxide with improved crystallinity and structural stability.

3.3 Morphological Analysis of WO_3 Films

The surface morphology of the deposited WO_3 films was analyzed using Scanning Electron Microscopy (SEM), as presented in **Figure 5**. **Figures 5(a), 5(b),** and **5(c)** show SEM images recorded at a magnification of 500× for films annealed at 500 °C, 600 °C, and 650 °C, respectively. Meanwhile, **Figure 5(d), 5(e),** and **5(f)** present SEM micrographs obtained at a higher magnification of 25,000× for the corresponding annealing temperatures.

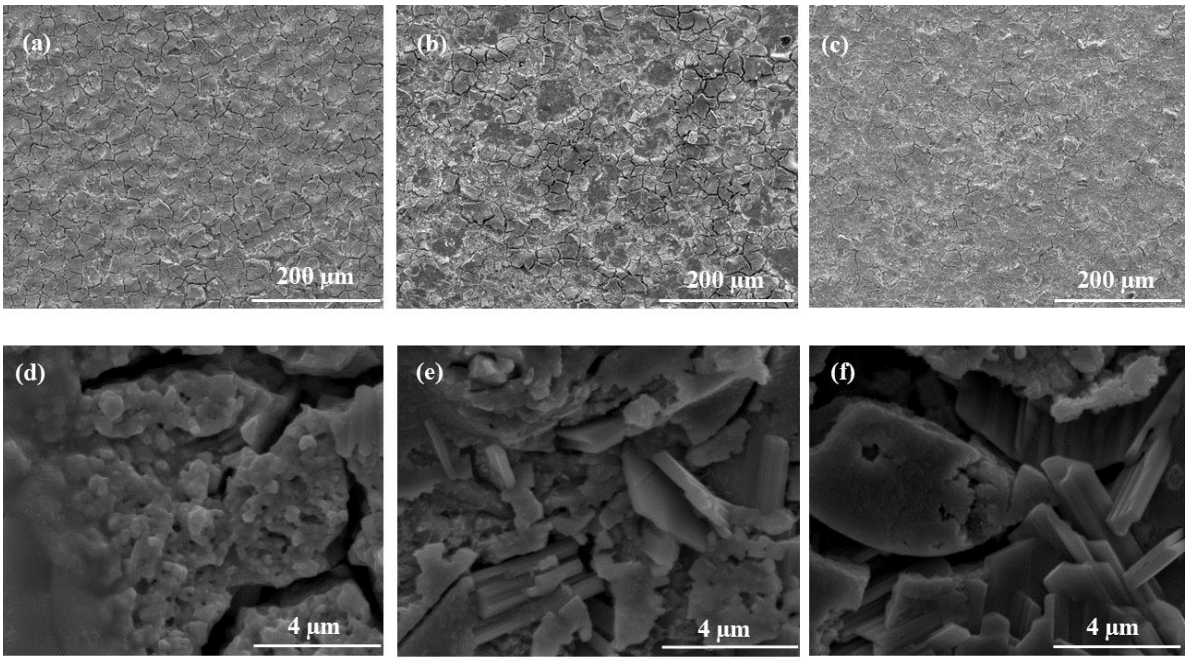

Figure 5. SEM images of WO_3 film morphology at 500× magnification: (a) 500 °C, (b) 600 °C, and (c) 650 °C; and at 25,000× magnification: (d) 500 °C, (e) 600 °C, and (f) 650 °C.

At low magnification (500×), all deposited WO_3 films successfully covered the glass substrate surface, indicating that the Direct Spray Deposition (DSD) method was capable of producing continuous films. However, differences in surface morphology were observed as the annealing temperature increased. The film annealed at 500 °C (**Figure 5.a**) exhibited a relatively rough and non-uniform surface with visible grain boundaries and microcrack-like features distributed across the film surface. This morphology suggests that the crystallization process was still incomplete at this temperature, consistent with the lower crystallinity observed in the XRD analysis. When the annealing temperature was increased to 600 °C (**Figure 5.b**), the surface became denser and more compact. The grain distribution appeared more homogeneous, although several interconnected crack patterns were still observed. The improved compactness of the film may be attributed to enhanced grain growth and particle coalescence during the annealing process. This observation is also in agreement with the XRD results, which showed sharper diffraction peaks and improved crystallinity at 600 °C. At 650 °C (**Figure 5.c**), the film surface appeared relatively smoother and more uniform compared to the films annealed at lower temperatures. The reduction in surface irregularities indicates that higher annealing temperatures promoted further crystal growth and structural rearrangement of the WO_3 film. The improved surface uniformity may also be associated with the formation of more thermodynamically stable tungsten oxide phases at elevated temperatures.

More detailed morphological evolution can be observed from the high-magnification SEM images (25,000×). The film annealed at 500 °C (**Figure 5.d**) showed agglomerated particles with irregular morphology and relatively small grain sizes. The particles appeared densely packed but lacked a well-defined crystal shape, indicating that crystal growth was still limited at this annealing temperature. At 600 °C (**Figure 5.e**), the morphology evolved into more distinct crystal structures with elongated and rod-like features. The particles became larger and more clearly defined, suggesting that higher thermal energy facilitated crystal growth and phase development. This morphological change corresponds well with the increased crystallinity observed in the XRD patterns. For the film annealed at 650 °C (**Figure 5.f**), plate-like structures became more dominant and clearly observable. The formation of these plate-like morphologies is consistent with previous studies reporting that higher annealing temperatures can promote anisotropic crystal growth in tungsten oxide materials (Hu et al., 2015; Raja et al., 2020). In addition, the larger crystal domains observed at this temperature indicate that grain growth became more significant during the annealing process. The annealing treatment not only contributed to crystal growth but also assisted in removing residual organic compounds originating from the precursor solution and surrounding atmosphere. Furthermore, the thermal treatment likely enhanced the adhesion and structural stability of the WO_3 films on the glass substrate. Overall, the SEM observations demonstrate that increasing the annealing temperature significantly influenced the surface morphology and microstructure evolution of the deposited WO_3 films.

4. Conclusions

WO_3 films were successfully immobilized on glass substrates using a combination of photodeposition and Direct Spray Deposition (DSD) methods. The XRD analysis demonstrated that the annealing temperature significantly influenced the crystal structure and phase composition of the deposited films. At 500 °C, the films were dominated by the W_5O_{14} phase with relatively low crystallinity, while increasing the annealing temperature to 600 °C and 650 °C promoted the formation of $W_{25}O_{73}$, $W_{18}O_{49}$, and WO_3 phases with improved crystallinity. SEM observations revealed that higher annealing temperatures also affected the surface morphology of the films, resulting in denser, more uniform, and well-defined structures. In particular, the film annealed at 650 °C exhibited the formation of plate-like

morphologies and larger crystal domains. Overall, the results indicate that the annealing temperature plays an important role in controlling the structural and morphological characteristics of WO_3 films prepared using the DSD method.

Acknowledgements

The authors sincerely acknowledge the research team and all institutions that contributed to the completion of this research. Their continuous support, insightful discussions, and constructive suggestions have significantly enhanced the quality and outcome of this work.

5. Bibliography

Acevedo-Peña, P., & González, I. (2014). Relation between morphology and photoelectrochemical performance of TiO_2 nanotube arrays grown in ethylene glycol/water. *Procedia Chemistry*, 12, 34–40. https://doi.org/10.1016/j.proche.2014.12.038

Arutanti, O., Sari, A. L., Kartikowati, C. W., Sari, A. A., & Arif, A. F. (2022). Design and application of homogeneous-structured TiO_2/activated carbon nanocomposite for adsorption–photocatalytic degradation of MO. *Water, Air, & Soil Pollution*, 233(4), Article 118. https://doi.org/10.1007/s11270-022-05600-1

Astuti, Y., Amri, D., Widodo, D. S., Widiyandari, H., Balgis, R., & Ogi, T. (2020). Effect of fuels on the physicochemical properties and photocatalytic activity of bismuth oxide synthesized using solution combustion method. *International Journal of Technology*, 11(1), 291–319. https://doi.org/10.14716/ijtech.v11i1.3342

Cao, X., Tao, J., Xiao, X., & Nan, J. (2018). Hydrothermal-assisted synthesis of the multi-element-doped TiO_2 micro/nanostructures and their photocatalytic reactivity for the degradation of tetracycline hydrochloride under visible light irradiation. *Journal of Photochemistry and Photobiology A: Chemistry*, 364, 202–207. https://doi.org/10.1016/j.jphotochem.2018.06.013

Hu, W.-H., Han, G.-Q., Dong, B., & Liu, C.-G. (2015). Facile synthesis of highly dispersed $WO_3{\cdot}H_2O$ and WO_3 nanoplates for electrocatalytic hydrogen evolution. *Journal of Nanomaterials*, 2015, Article 346086. https://doi.org/10.1155/2015/346086

Lee, J.-C., Gopalan, A.-I., Saianand, G., Lee, K.-P., & Kim, W.-J. (2020). Manganese and graphene included titanium dioxide composite nanowires: Fabrication, characterization and enhanced photocatalytic activities. *Nanomaterials*, 10(3), Article 456. https://doi.org/10.3390/nano10030456

Luo, N., Jiang, Z., Shi, H., Cao, F., Xiao, T., & Edwards, P. P. (2009). Photo-catalytic conversion of oxygenated hydrocarbons to hydrogen over heteroatom-doped TiO_2 catalysts. *International Journal of Hydrogen Energy*, 34(1), 125–129. https://doi.org/10.1016/j.ijhydene.2008.09.097

Murillo-Sierra, J. C., Hernández-Ramírez, A., Hinojosa-Reyes, L., & Guzmán-Mar, J. L. (2021). A review on the development of visible light-responsive WO_3-based photocatalysts for environmental applications. *Chemical Engineering Journal Advances*, 5, Article 100070. https://doi.org/10.1016/j.ceja.2020.100070

Nagarjuna, R., Challagulla, S., Sahu, P., Roy, S., & Ganesan, R. (2017). Polymerizable sol–gel synthesis of nano-crystalline WO_3 and its photocatalytic Cr(VI) reduction under visible light. *Advanced Powder Technology*, 28(12), 3265–3273. https://doi.org/10.1016/j.apt.2017.09.030

Raja, M., Chandrasekaran, J., Balaji, M., Kathirvel, P., & Marnadu, R. (2020). Influence of metal (M = Cd, In, and Sn) dopants on the properties of spin-coated WO_3 thin films and fabrication of temperature-dependent heterojunction diodes. *Journal of Sol-Gel Science and Technology, 93*(3), 495–505. https://doi.org/10.1007/s10971-019-05207-9

Sarteep, Z., Ebrahimian Pirbazari, A., & Aroon, M. A. (2016). Silver-doped TiO_2 nanoparticles: Preparation, characterization and efficient degradation of 2,4-dichlorophenol under visible light. *Journal of Water and Environmental Nanotechnology, 1*(2), 135–144. https://doi.org/10.7508/jwent.2016.02.007

Wang, C., Shao, C., Zhang, X., & Liu, Y. (2009). SnO_2 nanostructures–TiO_2 nanofibers heterostructures: Controlled fabrication and high photocatalytic properties. *Inorganic Chemistry, 48*(15), 7261–7268. https://doi.org/10.1021/ic9005983

Widiyandari, H., Firdaus, I., Purwanto, A., & Slamet, V. G. (2014). Synthesis of tungsten oxide (WO_3) film on glass substrate using aqueous-based solution spray deposition method. *Advanced Materials Research, 896*, 506–509. https://doi.org/10.4028/www.scientific.net/AMR.896.506

Widiyandari, H., Purwanto, A., Balgis, R., Ogi, T., & Okuyama, K. (2012). CuO/WO_3 and Pt/WO_3 nanocatalysts for efficient pollutant degradation using visible light irradiation. *Chemical Engineering Journal, 180*, 323–329. https://doi.org/10.1016/j.cej.2011.10.095

Xu, M., Gao, Y., Moreno, E. M., Kunst, M., Muhler, M., Wang, Y., Idriss, H., & Wöll, C. (2011). Photocatalytic activity of bulk TiO_2 anatase and rutile single crystals using infrared absorption spectroscopy. *Physical Review Letters, 106*(13), Article 138302. https://doi.org/10.1103/PhysRevLett.106.138302

Yu, J., Wang, Y., & Xiao, W. (2013). Enhanced photoelectrocatalytic performance of SnO_2/TiO_2 rutile composite films. *Journal of Materials Chemistry A, 1*(36), 10727–10735. https://doi.org/10.1039/C3TA12218B